The Contribution of Noise to Contrast Invariance of Orientation Tuning in Cat Visual Cortex

Jeffrey S. Anderson, Ilan Lampl, Deda C. Gillespie, David Ferster*

Feedforward models of visual cortex appear to be inconsistent with a well-known property of cortical cells: contrast invariance of orientation tuning. The models' fixed threshold broadens orientation tuning as contrast increases, whereas in real cells tuning width is invariant with contrast. We have compared the orientation tuning of spike and membrane potential responses in single cells. Both are contrast invariant, yet a threshold-linear relation applied to the membrane potential accurately predicts the orientation tuning of spike responses. The key to this apparent paradox lies in the noisiness of the membrane potential. Responses that are subthreshold on average are still capable of generating spikes on individual trials. Unlike the iceberg effect, contrast invariance remains intact even as threshold narrows orientation selectivity. Noise may, by extension, smooth the average relation between membrane potential and spike rate throughout the brain.

The width of orientation tuning of visual cortical neurons, as measured from their spike output, is invariant with contrast (*1*–*3*). The feedforward model of orientation selectivity proposed by Hubel and Wiesel (*4*), however, predicts approximate contrast invariance of orientation tuning not of spike responses, but of the synaptic input that simple cells receive from geniculate relay cells (*5*, *6*). Relay cell activity grows with increasing contrast, but because it is nearly orientation-independent, the membrane potential responses of postsynaptic cells should grow at all orientations. As a result, orientation tuning of the membrane potential responses should scale with contrast, without any change in width. In the presence of a fixed spike threshold (*7*), however, the orientation tuning of spike responses should widen with increasing contrast as more of the membrane potential tuning curve exceeds threshold (*8*).

In both simple (Fig. 1, A to E) and complex cells (Fig. 1, F to I), orientation tuning of both membrane potential and spike responses is contrast invariant (*9*). The red traces in (A) and (F) show an average (n = 5) of the membrane potential response to an optimally oriented stimulus of high contrast. This response is about twice as large as the response to a corresponding stimulus of low contrast (blue traces). From similar traces recorded at different orientations, we constructed orientation tuning curves for three different response measures: mean potential (C and H), mean spike rate (E and I), and, for simple cells, modulation of potential at the grating temporal frequency (D). Each tuning curve was then normalized to a peak amplitude of 1 and fitted to a Gaussian. In each cell, the fitted curves for the three contrasts were nearly identical in width. The iceberg effect (*7*) was also apparent: Spike tuning was narrower than membrane potential tuning, by ~50% in (E) and ~30% in (I). To quantify contrast invariance for the population, we plotted tuning widths derived from Gaussian fits at high and low contrast against one another for mean membrane potential and spikes (Fig. 1, J and K).

Figure 1 highlights an important feature of the cells that might underlie the contrast invariance of spike responses: Stimuli that evoked membrane potential responses whose average remained well below threshold nevertheless evoked reliable spiking. In Fig. 1, A and F, for example, the peak of the averaged response to the 8% contrast grating lies more than 5 mV below threshold, yet the tuning curve for spikes at 8% contrast (Fig. 1E) shows considerable activity. Furthermore, the contrast-response curve for spikes at the preferred orientation (Fig. 1, B and G) shows significant responses for contrasts as low as 4%. Yet in most cells, including those in Fig. 1, averaged membrane potential responses even at high contrast never exceeded spike threshold by more than a few millivolts, and in some cases never reached threshold at all.

The explanation for this behavior lies in the variability of the individual responses, as shown for another simple cell in Fig. 2. At the preferred orientation, the averaged response to high- and medium-contrast gratings consisted of a robust modulation of the membrane potential at the grating temporal frequency (Fig. 2A). At low contrast, the averaged response rose only slightly above baseline. Individual response trials (Fig. 2, B to D), however, offer a radically different picture. The maximum depolarization was similar at each contrast. What differed was the consistency of the responses and the relative time spent by the membrane potential above threshold. Thus, while the averaged responses suggested that low-contrast stimuli should evoke no spikes at all, the variability in individual responses clearly did trigger spikes (Fig. 2B), although at lower rates than would be expected from the medium and high contrasts. At the orthogonal orientation, the averaged membrane potential showed hardly any response, and few or no spikes were evoked.

The amplitude of the trial-to-trial variability in the responses (which we will refer to as "noise," although it need not be random) varied little with contrast and orientation (Fig. 2E). In 22 cells (Fig. 2G), we observed a 25 to 30% increase in noise at preferred orientations relative to orthogonal orientations (*10*), and a 10% decrease with increasing contrast. Noise at low frequencies (0.5 to 20 Hz) was nearly five times the noise at high frequencies (20 to 50 Hz) (Fig. 2H). Both low- and high-frequency components were elevated at preferred orientations relative to orthogonal orientations. Unlike low-frequency components, high-frequency components were elevated relative to rest at all orientations. Increases in contrast differentially affected low and high frequencies, decreasing low-frequency components by 10 to 25%, while elevating high-frequency components by 10 to 40%.

The response variability had the effect of smoothing the relation between averaged membrane potential and average firing rate (Fig. 2F), as compared with the threshold-linear relation between instantaneous membrane potential and firing rate (*11*). Even though the averaged membrane potentials for the highest contrast stimuli never exceed threshold (−65 mV), such stimuli evoked spikes: The averaged response combined with the noise was large enough to carry the membrane potential above threshold during some trials. The relation between average potential and firing rate could be approximated by a quadratic function, reminiscent of the squaring operation used to model cortical cells (*12*). Such a smoothing of the threshold nonlinearity preserves the contrast invariance of orientation tuning in the membrane potential responses as they are transduced into spikes, while at the same time narrowing the orientation tuning width. This can be best understood in the context of Fig. 1, D and E: To yield a close approximation to the Gaussian tuning curves of (E), one need only square the wider Gaussians of (D), reducing their widths by the square root of 2. This narrowing differs from a traditional iceberg effect: On

Department of Neurobiology and Physiology, Northwestern University, 2153 North Campus Drive, Evanston, IL 60208, USA.

*To whom correspondence should be addressed. E-mail: ferster@northwestern.edu

average, all stimuli that evoke a depolarization, no matter how small, still evoke an increase in spike rate.

We simulated the averaged responses of a simple cell to an optimal drifting grating (Fig. 3A) with sinusoidal modulations of the membrane potential superimposed on an increase in mean potential. The tuning curves of the membrane potential mean and modulation (Fig. 3B) were modeled by Gaussians of 30° half-width and amplitudes of 10-, 6-, and 3-mV peak-to-peak modulation, and 5-, 3- and 1.5-mV mean depolarization at the three different contrasts. Noise was simulated at each point in time by a normal probability distribution centered on the averaged potential. Spike rates were predicted from the integral of the probability curve multiplied by the threshold-linear function. The predicted tuning for spikes is shown for low noise (Fig. 3C) and for physiological levels of noise (Fig. 3D). The curves for the low-noise condition show marked changes in width with contrast; the curves for the high-noise condition show near perfect contrast invariance. The effects of changing the noise level are shown in Fig. 3E. Above a modest level of noise (2 to 3 mV), the tuning widths at each contrast converge toward a horizontal asymptote, such that increases in noise above this level change tuning width only slightly.

The effect of noise on tuning width was primarily generated at nonoptimal orientations. There, the variability was most needed to ensure that the membrane potential crossed spike threshold sufficiently to translate small membrane-potential responses into spike responses. As long as the noise was of sufficient amplitude at these orientations and contrasts, contrast invariance was predicted. The prediction of contrast invariance depended little on assumptions about the spectral composition or tuning properties of the noise. In the simulations shown, the noise was assumed to be untuned for contrast or orienta-

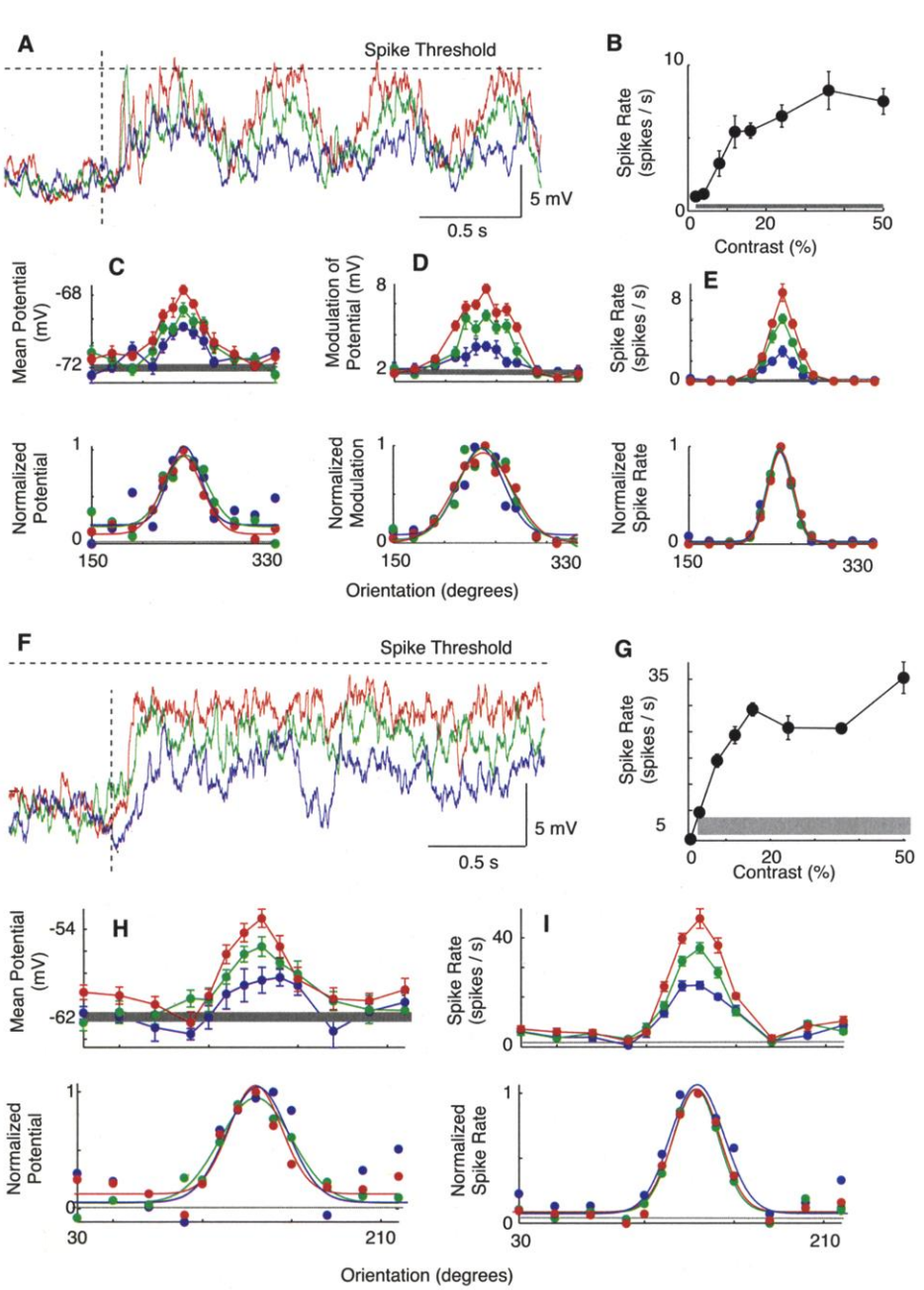

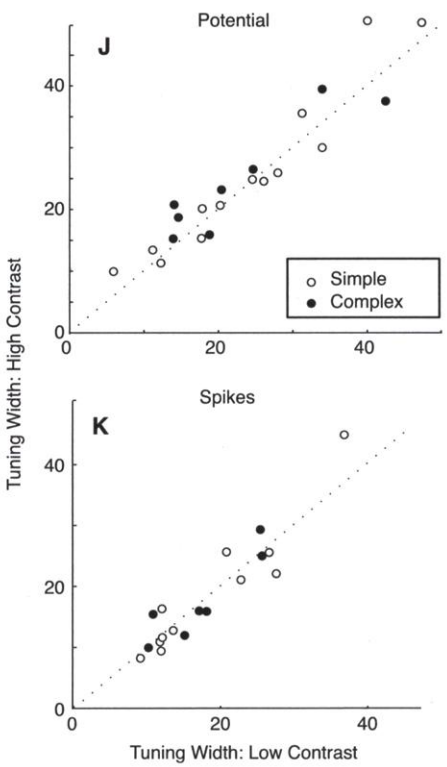

Fig. 1. Contrast invariance of orientation tuning. (**A**) Averaged membrane potential responses of a simple cell to optimally oriented gratings at 8% (blue), 20% (green), and 64% (red) contrast. Vertical dashed line represents stimulus onset. (**B**) Contrast-response curve for the same cell. Shaded region represents V_{rest} ± SEM. Error bars represent the SEM. (**C**) (Upper) Orientation tuning of mean potential at three contrasts. (Lower) The same tuning data normalized to a peak height of 1. Continuous curves are best fits to a Gaussian. (**D**) Orientation tuning of modulation of potential at the drift frequency of the stimulus. (**E**) Orientation tuning of spike rate. (**F** to **I**) Similar to (A) to (E) for a complex cell (modulation component of membrane potential omitted). (**J**) Orientation tuning widths at high (64%) versus low (8 to 16%) contrast of membrane potential across a population of 22 cells (mean for complex cells, ●; modulation for simple cells, ○). (**K**) Orientation tuning widths at high and low contrast of spike rate responses across a population of 18 reliably spiking cells. Dotted lines in (J) and (K) have a slope of 1.

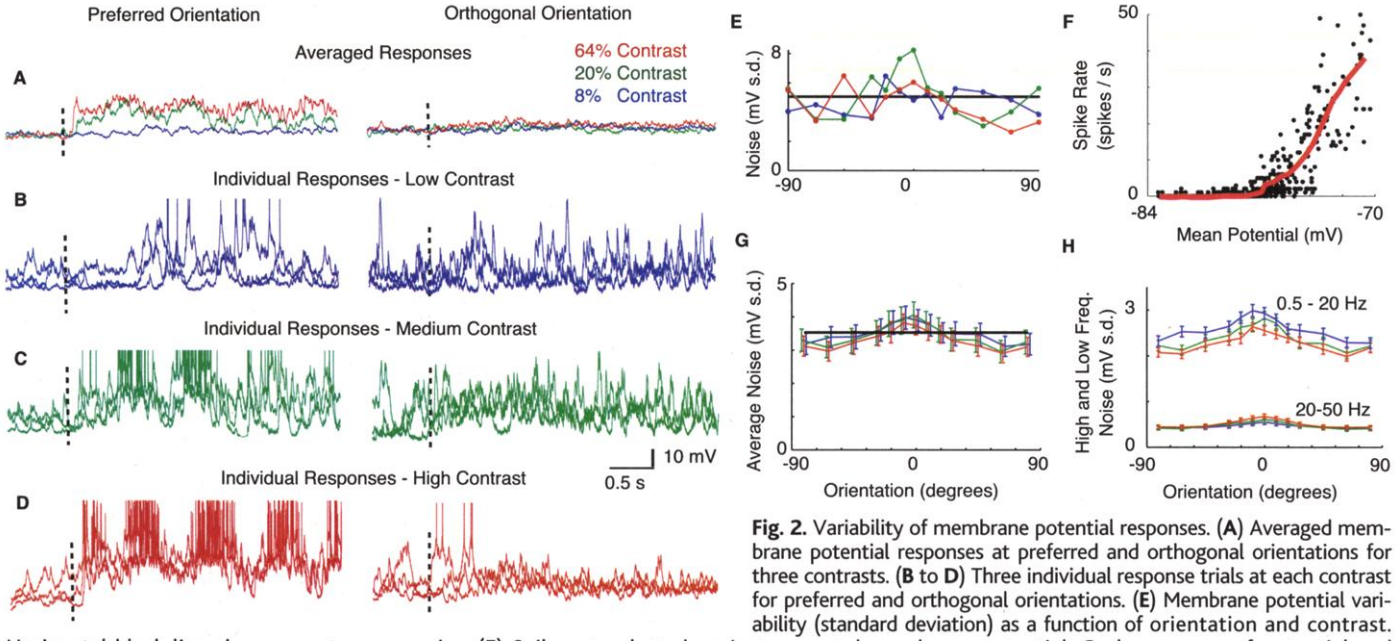

Fig. 2. Variability of membrane potential responses. (**A**) Averaged membrane potential responses at preferred and orthogonal orientations for three contrasts. (**B** to **D**) Three individual response trials at each contrast for preferred and orthogonal orientations. (**E**) Membrane potential variability (standard deviation) as a function of orientation and contrast. Horizontal black line shows spontaneous noise. (**F**) Spike rate plotted against averaged membrane potential. Cycle averages of potential and spikes for each orientation and each contrast were computed. Mean potential and spike rate were then plotted for each 10-ms interval in each cycle average. Red trace shows average of points for each membrane potential value. Spike threshold for this cell is −65 mV. (**G**) Noise amplitude (standard deviation) plotted against orientation at different contrasts averaged across 22 cells. Black line shows standard deviation of spontaneous noise in the population. (**H**) Same as (G) for low- (0.5 to 20 Hz) and high- (20 to 50 Hz) frequency components of the responses.

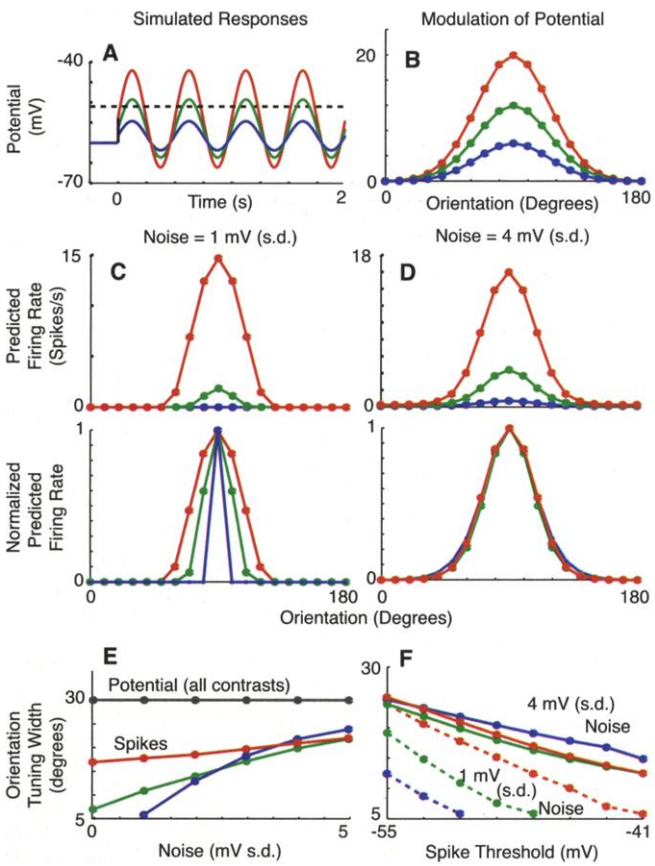

Fig. 3. Noise produces contrast invariance in a simulated simple cell. (**A**) Simulated membrane potential responses optimally oriented gratings at three different contrasts. Modulation amplitudes for the three different contrasts are 20, 12, and 6 mV. The dc offsets are 5, 3, and 1.5 mV. (**B**) Responses were tuned for orientation with a Gaussian of half-width at half height of 30°. (**C**) (Upper trace) Predicted spike tuning using threshold-linear model and low noise (1-mV SD). Threshold was −51 and slope of linear function was 6 spikes s^{-1} mV^{-1}. (Lower trace) Normalized tuning curves. (**D**) Predicted spike tuning using higher membrane-potential noise (4-mV SD). (**E**) Predicted spike tuning width as a function of noise for three different contrasts. Gray line, membrane potential tuning width. (**F**) Predicted spike tuning width as a function of spike threshold for three different contrasts (red, green, and blue) and for low and high noise (dashed and solid lines).

tion. Introducing a degree of tuning similar to that observed in Fig. 2, E and G, however, had no perceptible effect on the contrast invariance of the modeled responses (*13*).

As with recorded cells, the simulation showed a narrowing of tuning for spikes relative to the tuning of membrane potential (Fig. 3E). The effect gradually diminished with increases in noise, increased with distance between resting potential and spike threshold, but was largely independent of the position of spike threshold at high noise levels (Fig. 3F).

To determine whether the noise present in vivo could account for contrast invariance in spike orientation tuning, we applied the threshold-linear model of spiking to membrane potential traces recorded from 18 reliably spiking cells. Spikes rates were predicted with three different methods. First, we applied the threshold-linear model to the averaged responses (*14*). Second, we applied the model to individual response trials. Finally, we applied the model to the sum of the averaged responses and normally distributed noise of variance equal to that of the cell's spontaneous membrane potential. The resulting predicted tuning curves, together with measured tuning curves, are shown in Fig. 4 for one simple cell (A to D) and one complex cell (E to H). For both cells, orientation tuning is essentially contrast-invariant for all conditions except for predictions made from averaged responses without added noise. The same was true for the population, as shown in Fig. 4, I to K, where tuning widths at high and low contrast are compared for the three prediction methods. Unlike the noise recorded in cortical cells, which is dominated by low frequencies (Fig. 2H), the simulated noise used in Figs. 3 and 4, D and H, has equal components at all frequencies. Both realistic noise (Fig. 4, C and D) and spectrally flat noise, however, were able to predict contrast invariance in the spike output.

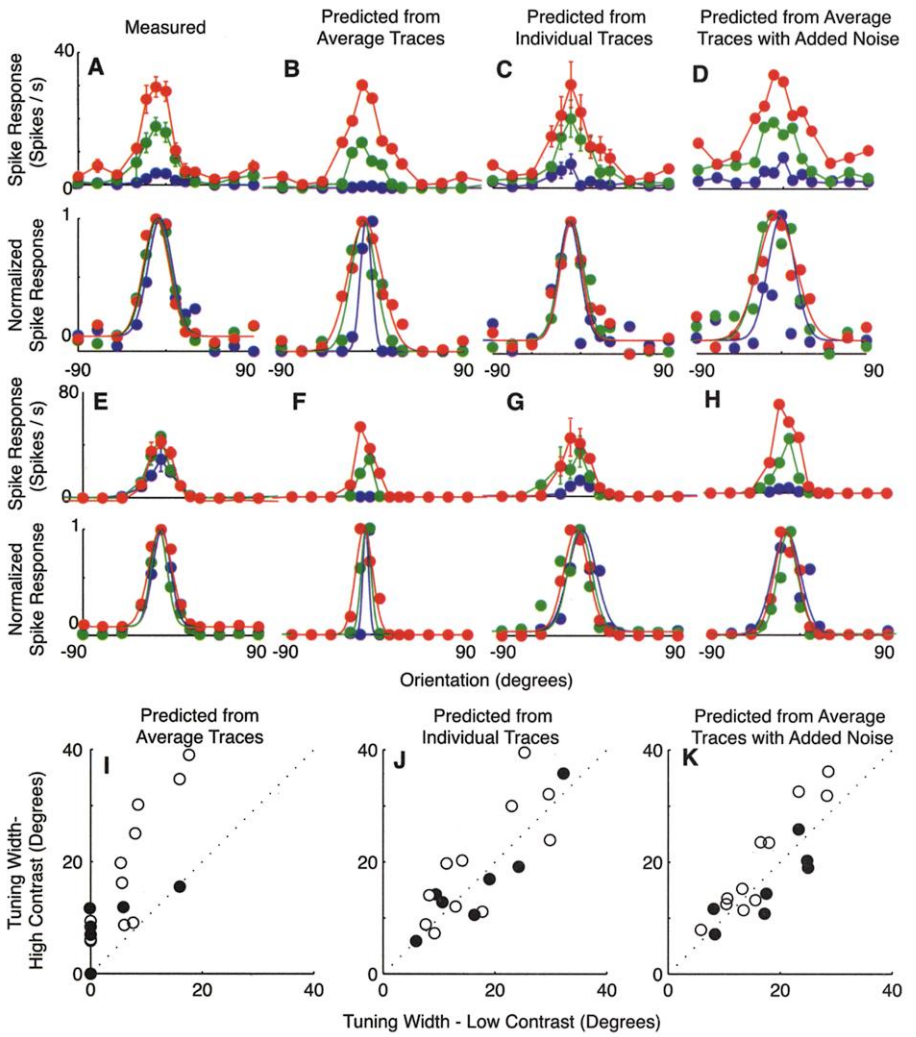

Fig. 4. Measured and predicted orientation tuning for spikes. (**A**) Measured spike orientation tuning at three contrasts (red, 64%; green, 20%; blue, 12%) for a simple cell. Error bars show ±SEM. (**B**) Spike orientation tuning predicted from averaged membrane potential responses. (**C**) Spike orientation tuning predicted from individual response trials. (**D**) Spike orientation tuning predicted from averaged responses with added noise. (**E** to **H**) Same as above for a complex cell. (**I**) Spike tuning width at high versus low contrast predicted from averaged membrane potential responses. Widths at high contrast were greater than at low contrast by 9.1° ± 1.2° (SEM, $n = 18$, $P < 0.001$; two-tailed t test). (**J**) Spike tuning width at high versus low contrast predicted from individual trials. (**K**) Spike tuning width at high versus low contrast predicted from averaged responses with added noise. Average difference in width at high and low contrasts was less that 1° in both (J) and (K).

Our findings partially solve the puzzle of how contrast invariance of orientation tuning arises in cortical cells. With sufficient noise, contrast-invariant tuning in membrane potential responses can generate contrast-invariant spike responses, despite nonlinear filtering by the spike threshold. But how does the orientation tuning of the membrane potential responses become contrast invariant? For cells (including most complex cells) that receive synaptic input of cortical origin, the answer is straightforward: Orientation tuning of the spike output of cortical cells is itself contrast-invariant (*1*–*3*). For cells (including most simple cells) that receive input from the lateral geniculate nucleus, the origin of contrast-invariant orientation tuning of synaptic inputs is more obscure. Hubel and Wiesel's model predicts that the mean component of the relay cell input grows with contrast at all orientations (*8*). That it fails to do so at null orientations (Fig. 1C) requires an additional or alternative mechanism to linear summation of thalamic inputs. One such mechanism is nonlinear, intracortical amplification of geniculate input by orientation-specific feedback connections (*15*–*17*). Alternatively, contrast-dependent, push-pull inhibition could counteract the rise in mean potential predicted to occur at orthogonal orientations (*6*).

Our data suggest that contrast invariance cannot be reliably achieved in a single cell for a single stimulus presentation. The reliable perception of stimulus orientation and contrast during a single trial seems to require averaging across a population of neurons. Population averages will only be effective, however, if the noise among individual cells (*18*) and their inputs (*19*, *20*) is uncorrelated, which is not always the case. Finally, our results suggest a more widespread function for noise. It allows the averaged membrane potential of a neuron to be translated into spiking in a smooth, graded manner across a wide range of potentials, starting far below threshold and continuing through threshold itself. Thus, cortical neurons exhibit a clear form of stochastic resonance in their responses to visual stimuli (*21*, *22*). With an appropriate level of noise, membrane potential responses evoked by low-contrast stimuli, which on average remain subthreshold, can nevertheless evoke significant spiking (*23*) that is entrained to the stimulus.

References and Notes

1. G. Sclar, R. D. Freeman, *Exp. Brain Res.* **46**, 457 (1982).
2. C. Li, O. Creutzfeldt, *Pflueg. Arch.* **401**, 304 (1984).
3. B. C. Skottun, A. Bradley, G. Sclar, I. Ohzawa, R. Freeman, *J. Neurophysiol.* **57**, 773 (1987).
4. D. H. Hubel, T. N. Wiesel, *J. Physiol.* (*London*) **160**, 106 (1962).
5. We refer to the tuning width relative not to the resting potential, but to the plateau of the tuning curve measured at orientations orthogonal to the preferred. The Hubel and Wiesel model predicts that this plateau might also grow with contrast in simple cells (*6*). We saw small increases in mean potential at orthogonal orientations in two of our simple cells, with corresponding increases in the mean firing rate. One such cell is shown in Fig. 4, A to D.
6. T. W. Troyer, A. E. Krukowski, N. J. Priebe, K. D. Miller, *J. Neurosci.* **18**, 5908 (1998).
7. M. Carandini, D. Ferster, *J. Neurosci.* **20**, 470 (2000); M. Volgushev, J. Pernberg, U. T. Eysel, *Eur. J. Neurosci.* **12**, 257 (2000).
8. D. Ferster, K. Miller, *Annu. Rev. Neurosci.* **23**, 441 (2000).
9. Recordings were obtained from anesthetized cats as described [S. Chung, D. Ferster, *Neuron* **20**, 1177 (1998)]. Visual stimuli consisted of sinusoidal gratings on a ViewSonic monitor (model PS 775; refresh rate, 120 Hz; mean luminance, 20 cd/ m^2) drifting at 2 Hz at optimal spatial frequency. Stimuli were generated by a Macintosh computer running Matlab with Psychophysics Toolbox extensions [D. H. Brainard, *Spat. Vision* **10**, 433 (1997); D. G. Pelli, *Spat. Vision* **10**, 437 (1997)]. For each cell, 2- to 4-s responses were recorded at three stimulus contrasts (64%; 20%; and 8, 12, or 16%) for 13 orientations, spaced at 20°-intervals from the preferred orientation, and presented 4 to 15 times in random order. Current-clamp recordings were made in the whole-cell configuration (6 cells) or with sharp microelectrodes (11 cells). Patch electrodes (4 to 13 megohm) were filled with (mM) 135 potassium gluconate, 5 Hepes, 2 $MgCl_2$, 1.1 EGTA, 0.1 $CaCl_2$, 3 adenosine triphosphate, 2 guanosine triphosphate, and 0.02 guanosine monophosphate (pH 7.4). Sharp electrodes (40 to 90 megohm) were filled with 2 M potassium acetate. Cells were classified as simple if receptive fields contained distinct on/off subfields. During two simple-cell recordings, a stimulating electrode was present in the ipsilateral lateral geniculate nucleus (LGN), and in both cases LGN stimulation produced excitatory postsynaptic potentials with latencies of 1.6 ms or less, indicative of monosynaptic geniculate input. Spikes were removed from all records by interpolation. Tuning widths are reported as half-width at half-height.

10. J. Anderson, I. Lampl, I. Reichova, M. Carandini, D. Ferster, *Nature Neurosci.* **3**, 617 (2000).
11. B. W. Knight, *J. Gen. Physiol.* **59**, 734 (1972).
12. D. J. Heeger, *Visual Neurosci.* **9**, 427 (1992).
13. We repeated the simulations illustrated in Fig. 3. Instead of using a constant-amplitude noise for all orientations and contrasts in the simulation, however, we used the values of Fig. 2G. The simulations resulted in contrast invariance indistinguishable from that shown in Fig. 3, E and F.
14. Spike threshold in the model, in some cases, was lowered below its measured value in order to obtain nonzero spike rates for predictions from averaged traces without added noise. In each cell, the same value for spike threshold was used for all three predictions.
15. D. C. Somers, S. B. Nelson, M. Sur, *J. Neurosci.* **15**, 5448 (1995).
16. R. Ben-Yishai, R. L. B. Or, H. Sompolinsky, *Proc. Natl. Acad. Sci. U.S.A.* **92**, 3844 (1995).
17. H. Sompolinsky, R. Shapley, *Curr. Opin. Neurobiol.* **7**, 514 (1997).
18. I. Lampl, I. Reichova, D. Ferster, *Neuron* **22**, 361 (1999).
19. J. M. Alonso, W. M. Usrey, R. C. Reid, *Nature* **383**, 815 (1996).
20. D. S. Reich, J. D. Victor, B. W. Knight, T. Ozaki, E. Kaplan, *J. Neurophysiol.* **77**, 2836 (1997).
21. A. Bulsara, E. W. Jacobs, T. Zhou, F. Moss, L. Kiss, *J. Theor. Biol.* **152**, 531 (1991).
22. K. Wiesenfeld, F. Moss, *Nature* **373**, 33 (1995).
23. N. Ho, A. Destexhe, *J. Neurophysiol.* **84**, 1488 (2000).
24. Supported by grant R01 EY04726 from the National Eye Institute. We thank K. D. Miller, T. W. Troyer, M. Stryker, and M. Carandini for valuable discussions.

13 September 2000; accepted 20 October 2000

Efficient Initiation of HCV RNA Replication in Cell Culture

Keril J. Blight,[1] Alexander A. Kolykhalov,[1] Charles M. Rice[1,2]*

Hepatitis C virus (HCV) infection is a global health problem affecting an estimated 170 million individuals worldwide. We report the identification of multiple independent adaptive mutations that cluster in the HCV nonstructural protein NS5A and confer increased replicative ability in vitro. Among these adaptive mutations were a single amino acid substitution that allowed HCV RNA replication in 10% of transfected hepatoma cells and a deletion of 47 amino acids encompassing the interferon (IFN) sensitivity determining region (ISDR). Independent of the ISDR, IFN-α rapidly inhibited HCV RNA replication in vitro. This work establishes a robust, cell-based system for genetic and functional analyses of HCV replication.

HCV (*1*) typically evades clearance by the host's immune system, allowing the establishment of a persistent infection in at least 70% of infected individuals. HCV-associated end-stage liver disease is now the leading cause of liver transplantation in the United States. Most patients treated with IFN alone either fail to respond or do not mount a sustained response. In Japanese patients, the amino acid sequence in a defined region of NS5A, designated the ISDR, appears to correlate with the effectiveness of IFN treatment. However, this association is substantially weaker or absent in patients infected with genotype 1a HCV strains or European patients infected with genotype 1b strains. Although considerable genetic heterogeneity exists among different HCV isolates, genotypes 1a and 1b are the most prevalent worldwide (*2*).

The single-stranded, positive-sense HCV RNA genome is ~9.6 kb in length and comprises a 5′ nontranslated region (NTR) that contains an internal ribosome entry site (IRES), a polyprotein coding region consisting of a single long open reading frame (ORF), and a 3′ NTR. Despite the availability of infectious cDNA clones [for examples, see (*3*, *4*)], efficient in vitro replication has not been observed. Recently, HCV replication was reported in the human hepatoma cell line, Huh7, after transfection of genotype 1b subgenomic RNA replicons expressing a selectable marker (*5*). These replicons contained (i) the HCV 5′ NTR fused to 12 amino acids of the capsid coding region; (ii) the neomycin phosphotransferase gene (Neo), which upon expression confers resistance to G418; (iii) the IRES from encephalomyocarditis virus (EMCV), which directs translation of HCV proteins NS2 or NS3 to NS5B; and (iv) the 3′ NTR. However, only 1 in 10^6 Huh7 cells supported HCV replication, which the authors attributed to low numbers of permissive cells (*5*).

To extend this system to other HCV genotypes, we constructed similar selectable replicons based on the HCV-H genotype 1a infectious clone (*3*). In contrast to the earlier study (*5*), we found that transfection of deoxyribonuclease (DNase)-treated RNA replicons (*6*, *7*) into multiple human hepatoma cell lines (*8*) failed to confer antibiotic resistance. The inability of the HCV-H–derived replicons to establish efficient HCV replication could indicate that the earlier success (*5*) was dependent on the particular genotype 1b consensus cDNA clone studied. As a positive control, we synthesized the genotype 1b replicon, I_{377}/NS3-3′ (*5*), using a polymerase chain reaction (PCR)–based gene assembly procedure (*9*) and transfected RNA transcripts into Huh7 cells (*6*, *7*). G418-resistant colonies supporting autonomous HCV replication (*10*) were observed at low frequency (*11*). In contrast, colonies were never observed for Huh7 cells electroporated in parallel with replicon RNA carrying a polymerase-defective lethal mutation in NS5B (pol$^-$) (*12*).

High-level replication may reflect a need for adaptation of the replicon to the host cell; hence, we sequenced uncloned reverse transcriptase (RT)–PCR products amplified from five independent G418-resistant cell clones (*13*). Each cell clone contained replicons with mutations in a defined region of NS5A; four clones contained replicons encoding amino acid substitutions upstream of the putative ISDR, and the fifth clone harbored a replicon encoding an in-frame deletion of 47 amino acids encompassing the ISDR. In addition to an amino acid change in NS5A, one replicon also encoded an amino acid substitution in NS3 and another encoded amino acid substitutions in both NS3 and NS4B (*14*). Sequence analysis of the NS5A coding region revealed that 12 of 17 additional cell clones had replicons with point mutations upstream of the ISDR (Fig. 1A). Thus, we identified nine different NS5A substitutions localizing to a region of about 30 amino acids, and a deletion of 47 amino acids (Fig. 1A).

We next engineered each change back into the I_{377}/NS3-3′ replicon. After transfection of mutant RNA transcripts into Huh7 cells and G418 selection (*6*, *7*), each construct established replication in 0.2 to 10% of transfected cells (Fig. 1A), as compared with 0.0005% for the original I_{377}/NS3-3′ replicon. Hence, each of the 10 mutations in NS5A enhanced the ability of HCV replicons to replicate. Engineering the Δ47aa and S1179I mutations into the HCV-H genotype 1a–derived replicon did not result in detectable replication in Huh7 cells. This suggests that different or additional adaptive mutations may be required for RNA replication of other isolates.

To examine the ability of these mutant constructs to replicate over a shorter time scale in the absence of G418 selection, we measured HCV-specific RNA amplification at different times after transfection. Replicons with the highest transduction efficiency displayed the greatest level of HCV RNA accumulation in this first cycle assay (Fig. 1B). For the replicon S1179I, HCV RNA levels increased to ~20-, 300-, and 400-fold relative to the pol$^-$ negative control at 24, 48, and 96 hours, respectively (Fig. 1B).

[1]Department of Molecular Microbiology, Washington University School of Medicine, 660 South Euclid Avenue, St. Louis, MO 63110–1093, USA. [2]Center for the Study of Hepatitis C, Rockefeller University, Box 64, 1230 York Avenue, New York, NY 10021, USA.

*To whom correspondence should be addressed. E-mail: ricec@rockvax.rockefeller.edu